

Intergalactic medium dispersion measures of fast radio bursts estimated from IllustrisTNG simulation and their cosmological applicationsZ. J. ZHANG,¹ K. YAN,¹ C. M. LI,¹ G. Q. ZHANG,¹ AND F. Y. WANG^{1,2}¹*School of Astronomy and Space Science, Nanjing University, Nanjing 210093, China*²*Key Laboratory of Modern Astronomy and Astrophysics (Nanjing University), Ministry of Education, Nanjing 210093, China***ABSTRACT**

Fast radio bursts (FRBs) are millisecond-duration radio transients and can be used as a cosmological probe. However, the dispersion measure (DM) contributed by intergalactic medium (IGM) is hard to be distinguished from other components. In this paper, we use the IllustrisTNG simulation to realistically estimate the DM_{IGM} up to $z \sim 9$. We find $DM_{\text{IGM}} = 892^{+721}_{-270}$ pc cm⁻³ at $z = 1$. The probability distribution of DM_{IGM} can be well fitted by a quasi-Gaussian function with a long tail. The tail is caused by the structures along the line of sight in IGM. Subtracting DM contributions from the Milky Way and host galaxy for localized FRBs, the DM_{IGM} value is close to the derived $DM_{\text{IGM}} - z$ relation. We also show the capability to constrain the cosmic reionization history with the DM_{IGM} of high-redshift FRBs in the IllustrisTNG universe. The derived $DM_{\text{IGM}} - z$ relation at high redshifts can be well fitted by a *tanh* reionization model with the reionization redshift $z = 5.95$, which is compatible with the reionization model used by the IllustrisTNG simulation. The DM_{IGM} of high-redshift FRBs also provides an independent way to measure the optical depth of cosmic microwave background (CMB). Our result can be used to derive the pseudo-redshifts of non-localized FRBs for $DM_{\text{IGM}} < 4000$ pc cm⁻³.

Keywords: radio bursts; intergalactic medium; reionization**1. INTRODUCTION**

Fast radio bursts (FRB) are millisecond luminous radio pulses with large dispersion measures (DMs), well in excess of the Milky Way contribution. There have been more than one hundred FRBs reported since Lorimer et al. (2007) found the first one from archival data. Among them, only thirteen FRBs have been localized (Chatterjee et al. 2017; Bannister et al. 2019; Ravi et al. 2019; Prochaska et al. 2019; Marcote et al. 2020; Macquart et al. 2020). Apparently, FRBs can be divided into two types, repeating and non-repeating ones and their host galaxy properties may be different.

The DM is defined as the column density of free electron density along a given line of sight (LoS). The observed DM is usually divided into several parts

$$DM = DM_{\text{MW}} + DM_{\text{halo}} + DM_{\text{IGM}} + \frac{DM_{\text{host}} + DM_{\text{source}}}{1 + z}. \quad (1)$$

In the above equation, DM_{MW} is the contribution of the interstellar medium in the Milky Way, which can be derived from the NE2001 Galactic free electron density model (Cordes & Lazio 2002) or the YMW model (Yao et al. 2017). DM_{halo} is contributed by the free electrons in the Galactic halo. Prochaska & Zheng (2019) found that the DM_{halo} is $50 \text{ pc cm}^{-3} < DM_{\text{halo}} < 80 \text{ pc cm}^{-3}$. Recently, Yamasaki & Totani (2020) estimated that the mean DM_{halo} is 43 pc cm^{-3} , with a full range of $30\text{--}245 \text{ pc cm}^{-3}$. Zhang et al. (2020) derived host contribution DM_{host} distributions of repeating and non-repeating FRBs with the IllustrisTNG simulation. They found that the distributions of DM_{host} can be well fitted by a log-normal function. For non-repeating FRBs, the median of DM_{host} is about $30\text{--}70 \text{ pc cm}^{-3}$ in the redshift range $z = 0.1\text{--}1.5$. The DM_{source} depends on the central engine of FRBs. If FRB is generated by mergers of binary neutron stars (Wang et al. 2016; Zhang 2020), the value of DM_{source} is small (Wang et al. 2020; Zhao et al. 2020).

The DM contributed by intergalactic medium (IGM) is an important cosmological probe (Zhou et al. 2014; Gao et al. 2014; Muñoz et al. 2016; Yu & Wang 2017;

Wang & Wang 2018; Walters et al. 2018; Jaroszynski 2019; Wei et al. 2019; Li et al. 2019; Wu et al. 2020; Zhao et al. 2020). By assuming the cosmic reionization history, the value of DM_{IGM} can be derived theoretically from (Ioka 2003; Inoue 2004; Deng & Zhang 2014)

$$DM_{\text{IGM}}(z) = \frac{3c\Omega_b H_0}{8\pi G m_p} \int_0^z \frac{(1+z') f_{\text{IGM}}(z') f_e(z')}{E(z')} dz', \quad (2)$$

where $E(z) = H(z)/H_0$, $H(z)$ is Hubble parameter, H_0 is the Hubble constant, m_p is the mass of proton, $\Omega_b = 0.0486$ is the density of baryons, and f_{IGM} is the fraction of baryon mass in the IGM. $f_e = Y_{\text{H}} X_{\text{e,H}}(z) + \frac{1}{2} Y_{\text{He}} X_{\text{e,He}}(z)$. $Y_{\text{H}} = 3/4$ and $Y_{\text{He}} = 1/4$ are the mass fractions of hydrogen and helium, respectively. $X_{\text{e,H}}$ and $X_{\text{e,He}}$ are the ionization fractions of intergalactic hydrogen and helium.

Different from the previous theoretical investigations which use extragalactic DM with a homogeneous universe (Ioka 2003; Inoue 2004), McQuinn (2014) considered the effect of inhomogeneity with three models for halo gas profile of the ionized baryons. Dolag et al. (2015), Pol et al. (2019) and Zhu & Feng (2020) studied DM_{IGM} with different cosmological simulations at low-redshift ($z < 2$) universe. Jaroszynski (2019) used the Illustris simulation to estimate the DM_{IGM} and its scatters in the $z < 5$ universe. However, the simulation accuracy can be improved with the latest IllustrisTNG simulation. Another advantage of IllustrisTNG is that it can provide the electron density directly instead of converting from the dark matter particle number density to baryonic matter density like Pol et al. (2019). The complicated conversion may bring in extra uncertainties. Besides, the IllustrisTNG has a wide redshift range.

Considering these advantages, we choose the IllustrisTNG (the successor of Illustris) simulation which possesses both the high accuracy and large structures in the range $0 < z < 20$. Such a broad range of redshifts enables us to examine the prospect of constraining the cosmic reionization history with high-redshift FRBs. It also gives a chance to check whether FRBs can be a new type of standard candles besides supernovae, which is crucial for distance measurement.

In this paper, we use the IllustrisTNG simulation to study DM_{IGM} and their cosmological applications, especially at the high-redshift universe. The outline is as follows. An introduction to the IllustrisTNG simulation and our method to derive DM_{IGM} from the simulation are given in Section 2. We show the result in Section 3. The scenario of constraining the cosmic reionization history with FRBs is discussed in Section 4. We estimate the redshifts of non-localized FRBs with $DM_{\text{IGM}} - z$

relation in Section 5. Conclusions are given in Section 6.

2. METHODS

2.1. Data access to IllustrisTNG

The IllustrisTNG project, a successor of Illustris, consists of three large volume, cosmological and gravo-magnetohydrodynamical simulations (Pillepich et al. 2018; Springel et al. 2018; Nelson et al. 2018; Marinacci et al. 2018; Naiman et al. 2018), such as TNG50, TNG100, and TNG300. The number represents the scale of simulations in the unit of cMpc (c for comoving similarly hereinafter). Each simulation contains several runs with different resolutions. The final results are stored in 600 HDF5 files. According to the cosmological principle, TNG300 is the best choice for our research and TNG300-1 is chosen among the three runs for its best resolution. There are 100 snapshots at different redshifts stored in each run and each snapshot has 15,625,000,000 Voronoi gas cells in total. Each cell corresponds to a particle and its physical parameters given by IllustrisTNG represent the whole cell. In the 100 snapshots, 20 snapshots are ‘full’ and 80 snapshots are ‘mini’ which only lack some particle fields. We use all the full snapshots at $z < 10$ and several ‘mini’ snapshots for better accuracy. The web-based JupyterLab Workspace and high-performance computing resources provided by IllustrisTNG are used in this work.

2.2. Dispersion of IGM

For an FRB at z_s , the DM_{IGM} can be written as

$$DM_{\text{IGM}}(z_s) = \int_0^{z_s} \frac{n_e(z)}{1+z} dl_{\text{prop}}, \quad (3)$$

where $n_e(z)$ is electron density in the comoving frame and dl_{prop} is the differential proper distance. Then we use the redshift differential dz to express dl_{prop} as

$$dl_{\text{prop}} = \frac{c}{H_0(1+z)E(z)} dz, \quad (4)$$

where

$$E(z) = \sqrt{\Omega_m(1+z)^3 + \Omega_k(1+z)^2 + \Omega_\Lambda}. \quad (5)$$

So the DM_{IGM} can be rewritten as

$$DM_{\text{IGM}}(z_s) = \frac{c}{H_0} \int_0^{z_s} \frac{n_e(z)}{(1+z)^2 E(z)} dz. \quad (6)$$

The cosmological parameters are taken as $\Omega_m = 0.3089$, $\Omega_\Lambda = 0.6911$, and $H_0 = 67.74 \text{ km s}^{-1} \text{ Mpc}^{-1}$, which are the same as those used by the IllustrisTNG simulation (Pillepich et al. 2018).

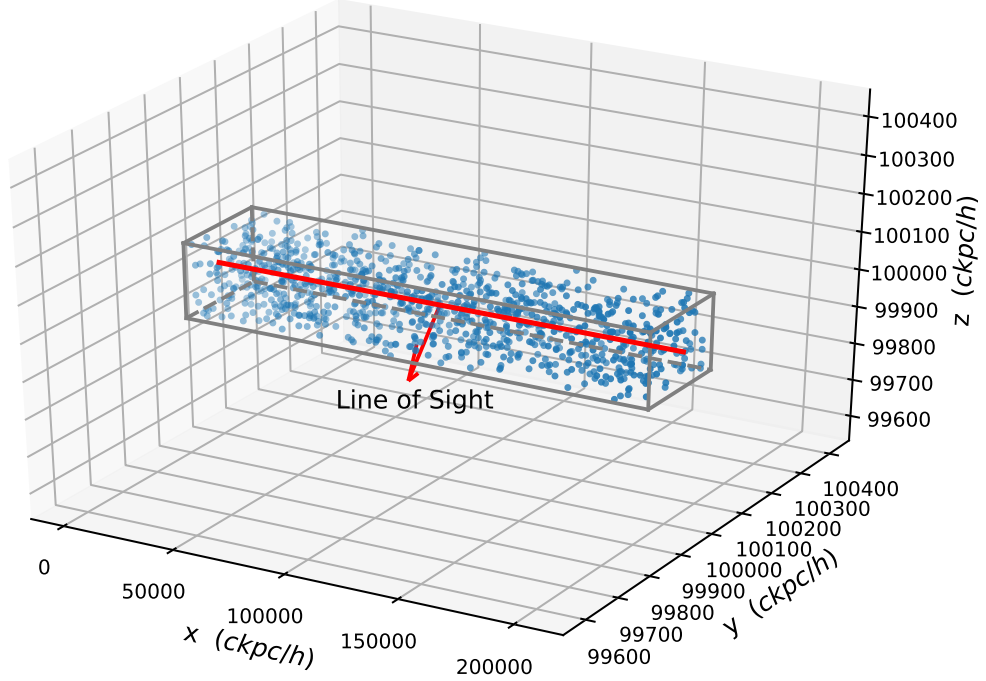


Figure 1. A schematic diagram of choosing LoS. There are 5125 pipes at each redshift as shown in this figure.

None of cosmological simulations provides continuous universe evolution, that's why snapshots exist. Therefore, equation (6) cannot be applied directly. In practice, Jaroszynski (2019) and Pol et al. (2019) clipped and stacked the snapshots to construct the LoS. Here we solve the problem from another aspect. The basic idea is to convert the integral into summation.

If $n_e(z_i)$ is available, the dDM_{IGM}/dz at a specific redshift z_i ($z_i = 0, 0.1, 0.2, 0.3, 0.4, 0.5, 0.7, 1, \dots$) can be derived by

$$\left. \frac{dDM_{\text{IGM}}}{dz} \right|_{z=z_i} = \frac{c}{H_0} \frac{n_e(z_i)}{(1+z_i)^2 E(z_i)}, \quad (7)$$

Then we use

$$DM_{\text{IGM}}(z_{i+1}) = DM_{\text{IGM}}(z_i) + \frac{1}{2} \left(\left. \frac{dDM_{\text{IGM}}}{dz} \right|_{z_i} + \left. \frac{dDM_{\text{IGM}}}{dz} \right|_{z_{i+1}} \right) (z_{i+1} - z_i) \quad (8)$$

to calculate the DM_{IGM} with the initial condition $DM_{\text{IGM}}(z)|_{z=0} = 0$. Next subsection will introduce how to obtain the electron density.

2.3. Calculations of DM_{IGM}

IllustrisTNG snapshot data is not organized according to spatial position. In order to obtain the average electron density along a given LoS, we use a traversal method on all the 15,625,000,000 particles and find

the particles belonging to the given LoS. For computational simplicity, the LoS is chosen to parallel to the x axis, which is similar to Jaroszynski (2019). Then we make 5125 square pipes with 200 ckpc/h ($H_0 = 100 h \text{ km s}^{-1} \text{ Mpc}^{-1}$) side in each snapshot and find the particles as well as necessary parameters (including *Coordinates*, *Density*, *ElectronAbundance*, *GFM_Metals* and *StarFormationRate*) in the pipes (see Figure 1). The 5125 pipes are chosen from different locations at 24 snapshots randomly and K-S test shows the sample size is representative. The electron density can be calculated by

$$n_e(z)_{\text{prop}} = \eta_e X_H \frac{\rho}{m_p} (1+z)^3, \quad (9)$$

where η_e is the electron abundance, X_H is the hydrogen mass abundance, ρ is the density and m_p is mass of a hydrogen atom. The fourth parameter is the particle coordinate, which is used to select particles. The factor $(1+z)^3$ converts the density in the simulation comoving units into the proper units.

The equation (9) cannot be used in star-forming gas because the calculation is based on the 'effective' temperature of the equation of state, which is not a physical temperature¹. Therefore, we use the parameter *StarFormationRate* to exclude the star-forming gas. For

¹ <https://www.tng-project.org/data/docs/specifications/>

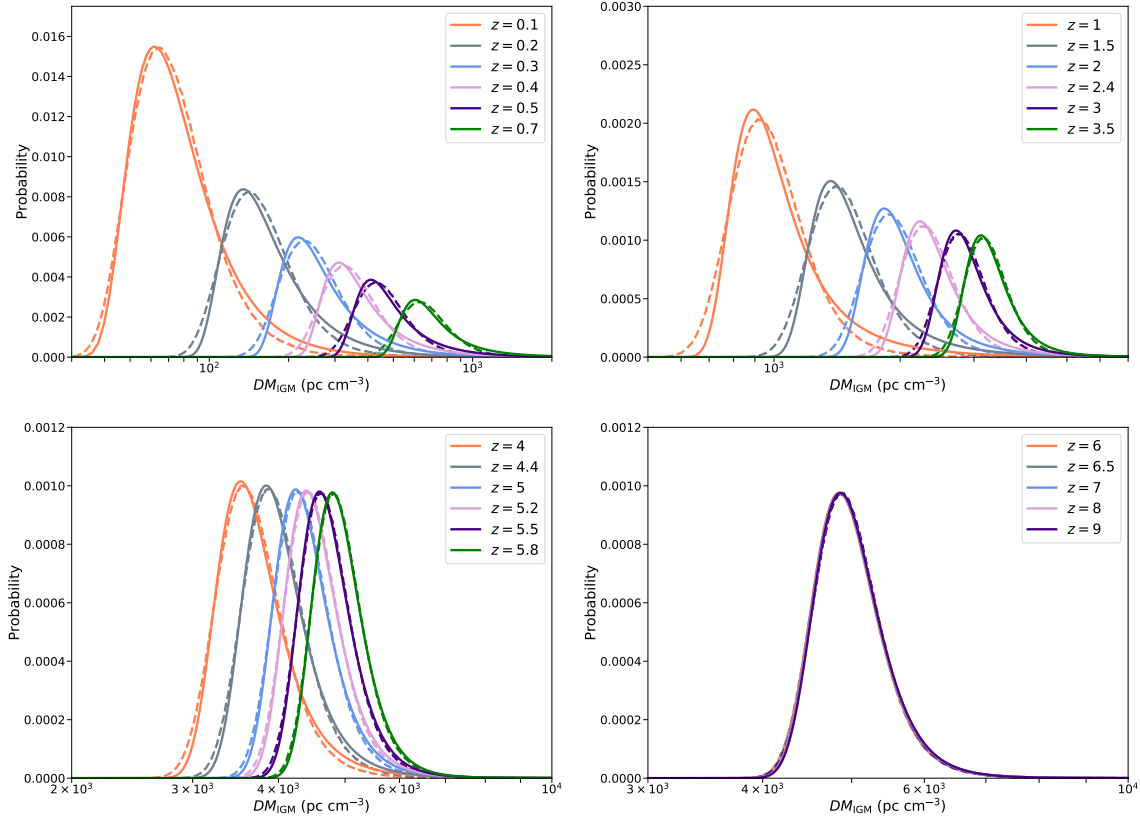


Figure 2. DM_{IGM} distributions from $z = 0.1$ to 9. Dashed lines are DM_{IGM} distributions derived from IllustrisTNG simulations and solid lines are the fitting results using equation (10). The best fitting parameters are shown in Table 1. At $z > 6$, the distributions overlap as shown in panel (e), which indicates the universe do not reionize at such high redshifts.

comparison, star-forming particles are also excluded in Dolag et al. (2015). Jaroszynski (2019) excluded gas cells belonging to haloes where dark matter density is 15 times larger than the cosmic critical density.

It is hard to get the electron density field along the LoS analytically, which requires to calculate the boundary of all the cells. While we know the cell to which any point on a LoS belongs. We divide the pipe into 10,000 bins along the x axis and take the geometric center coordinates as the representation of bins. The distances between each bin and each particle in the pipe are calculated. We choose the nearest particle of each bin and assume the bin belongs to the cell of the chosen particle. We take an average of the electron density of 10,000 bins and put it into equation (7). As a result, 5125 dDM_{IGM}/dz are obtained at each redshift. Ten million $DM_{\text{IGM}} - z$ relations are built by randomly selected dDM_{IGM}/dz from $z = 0.1$ to 9.

3. RESULT

The redshifts of snapshots besides $z = 0$ are shown in Table 1. The distributions of DM_{IGM} (from 0 to z similarly hereafter) at different redshifts are shown in Figure 2. The DM distributions are fitted with (McQuinn 2014; Prochaska & Zheng 2019; Macquart et al. 2020):

$$p_{\text{IGM}}(\Delta) = A\Delta^{-\beta} \exp\left[-\frac{(\Delta^{-\alpha} - C_0)^2}{2\alpha^2\sigma_{\text{DM}}^2}\right], \Delta > 0, \quad (10)$$

where $\Delta = DM_{\text{IGM}} / \langle DM_{\text{IGM}} \rangle$, and β is related to the inner density profile of gas in halos. We take $\alpha = \beta = 3$, which is the same as Macquart et al. (2020). σ_{DM} is an effective standard deviation. C_0 , which can affect the horizontal position, is the remaining parameter to be fitted. The fitting results are shown in Table 1.

It's obvious that the asymmetrical distributions have long tails at high DM_{IGM} , so we choose the most probable value for analysis, which is also used by Dolag et

z	A	C_0	σ_{DM}
0.1	0.04721	-13.17	2.554
0.2	0.005693	-1.008	1.118
0.3	0.003584	0.596	0.7043
0.4	0.002876	1.010	0.5158
0.5	0.002423	1.127	0.4306
0.7	0.001880	1.170	0.3595
1	0.001456	1.189	0.3044
1.5	0.001098	1.163	0.2609
2	0.0009672	1.162	0.2160
2.4	0.0009220	1.142	0.1857
3	0.0008968	1.119	0.1566
3.5	0.0008862	1.104	0.1385
4	0.0008826	1.092	0.1233
4.4	0.0008827	1.084	0.1134
5	0.0008834	1.076	0.1029
5.2	0.0008846	1.073	0.09918
5.5	0.0008863	1.070	0.09481
5.8	0.0008878	1.067	0.09072
6	0.0008881	1.066	0.08971
6.5	0.0008881	1.066	0.08960
7	0.0008881	1.066	0.08952
8	0.0008881	1.066	0.08944
9	0.0008881	1.066	0.08941

Table 1. Redshifts of the snapshots and fitting parameters of the DM_{IGM} distributions in Figure 2.

al. (2015) and Pol et al. (2019). We find $DM_{\text{IGM}}(z = 1) = 892_{-270}^{+721}$ pc cm⁻³ (errors represent 95% confidence level). Ioka (2003) and Inoue (2004) predicted $DM_{\text{IGM}}(z = 1) \sim 1200$ pc cm⁻³. Zhang (2018) predicted $DM_{\text{IGM}}(z = 1) \sim 855 \pm 345$ pc cm⁻³. Jaroszynski (2019) found $DM_{\text{IGM}}(z = 1) \sim 905 \pm 115$ pc cm⁻³ (errors represent 1σ standard deviation). Pol et al. (2019) derived $DM_{\text{IGM}}(z = 1) \sim 800_{-170}^{+7000}$ pc cm⁻³ with uniform weighting and $DM_{\text{IGM}}(z = 1) \sim 960_{-160}^{+350}$ pc cm⁻³ with weighting by matter distribution (errors represent 95% confidence level). In Figure 3, we show these above $DM_{\text{IGM}} - z$ relations. Our result is shown as blue solid line with 95% confidence region (blue region). The DM_{IGM} estimated in our work is consistent with others within 95% confidence level including the one derived by Pol et al. (2019). The difference between Pol et al. (2019) and our result may be caused by the conversion from the dark matter number density to the free electron density in the MareNostrum Instituto de Ciencias del Espacio Onion Universe simulation. A non-negligible systematic error may be from the different cosmological parameters used by these simulations. For example, Illustris uses the cosmological parameters from WMAP-9 measurements (Vogelsberger et al. 2014),

while IllustrisTNG uses those from *Planck* (Pillepich et al. 2018).

We also compare our result with several localized FRBs (Bannister et al. 2019; Ravi et al. 2019; Prochaska et al. 2019; Macquart et al. 2020) in Figure 4. The blue line is our result derived from TNG300 and the blue shade region is the 95% confidence region. The theoretical one from equation (2) is shown as dash line for the cosmological parameters from Planck (Planck Collaboration et al. 2016). The DM_{host} value is adopted from Zhang et al. (2020). Based on the host galaxy observations, Zhang et al. (2020) calculated the DM_{host} of repeating and non-repeating FRBs from the IllustrisTNG simulation. They found $DM_{\text{host}} = 32.97(1+z)^{0.84}$ pc cm⁻³ for non-repeating FRBs. For FRB 190608 we adopt its $DM_{\text{host}} = 137 \pm 43$ pc cm⁻³ from observations (Chittidi et al. 2020). The DM_{MW} value is derived with the NE2001 model (Cordes & Lazio 2002). We take $DM_{\text{halo}} = 50$ pc cm⁻³ for all FRBs. The contributions from FRB sources are ignored. All the derived DM_{IGM} are compatible with our result.

4. THE SCENARIO OF CONSTRAINING THE COSMIC REIONIZATION HISTORY

High-redshift FRBs can be used to probe the cosmic reionization history and we test the expectation with TNG300 simulation. The universe is mostly neutral and non-transparent after the recombination (Peebles 1968; Zel'dovich et al. 1969; Seager et al. 2000). The transition from the neutral to ionized universe called reionization, which is the first chance to detect the universe evolution after the end of cosmic dark ages. Reionization history is a frontier and challenging area in cosmology (Loeb & Furlanetto 2013), because it is hard to detect now. Usually, it is believed that the reionization of hydrogen occurs between $z \sim 12$ and $z \sim 6$. For helium the range is between $z \sim 6$ and $z \sim 2$ (Planck Collaboration et al. 2016). Some works have proposed to use the FRBs to constrain the reionization history (Zheng et al. 2014; Fialkov & Loeb 2016; Linder 2020; Dai & Xia 2020; Bhattacharya et al. 2020).

It is still difficult to localize non-repeating FRBs even at low redshifts. The capability of localization is improving. Leung et al. (2020) demonstrated that the blind interferometric detection and localization of non-repeating FRBs by the CHIME and the CHIME Pathfinder can be down to about milliarcsecond precision. In future, they will observe thousands of single FRB events to this precision. However, considering the offsets which have been observed in FRBs, spectroscopy should be applied for high-redshift FRBs besides radio interferometer. To confirm the redshift, optical/infrared obser-

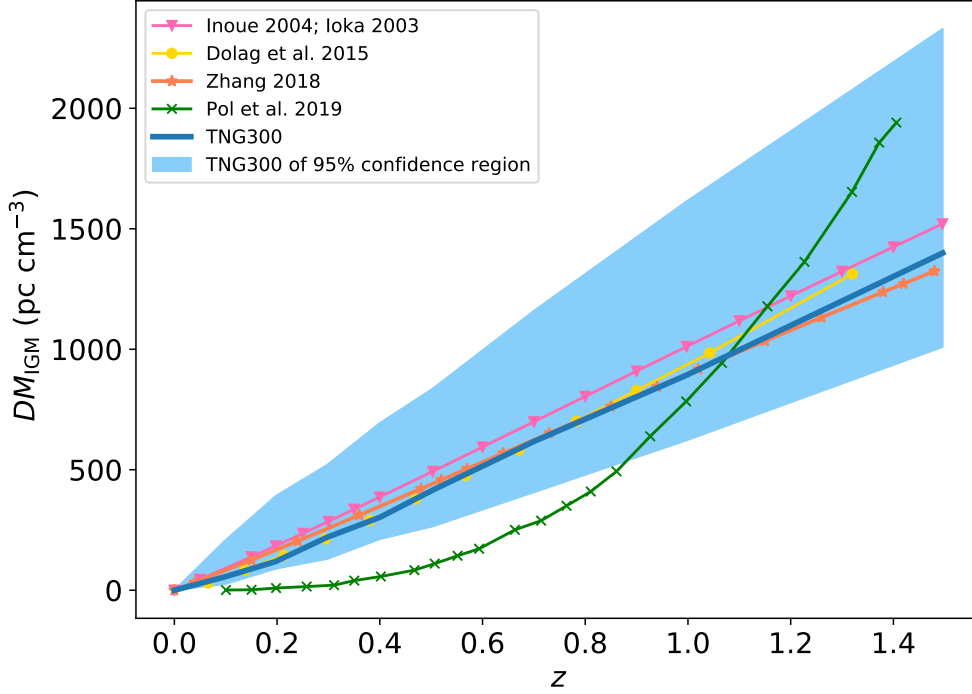


Figure 3. $DM_{\text{IGM}} - z$ relation at low redshift ($z < 1.5$). The blue line is our result from IllustrisTNG simulation and the blue shaded region is the 95% confidence region. Other results are shown for comparison. The pink line with inverted triangle markers is taken from Ioka (2003) and Inoue (2004). The dotted yellow line is taken from Dolag et al. (2015), the orange line with star marker is taken from Zhang (2018) and the green line with cross marks is Pol et al. (2019) uniform weighting result. Our result is consistent with other works except for the result of Pol et al. (2019). However, if considering the large confidence level of Pol et al. (2019) (not shown in this figure), our result is consistent with theirs.

variations should also be applied. Finding high-redshift quasars is a challenging task at present, let alone the high-redshift FRB hosts which may be faint.

Combining the high burst rate and the construction of next generation telescopes, it is hopeful to constrain the reionization history with FRBs. The estimated $\gtrsim 10^3 \text{ day}^{-1}$ rate of FRBs (Petroff et al. 2019) would provide abundant chances for future detections. Although the redshift distribution of FRBs is unknown, it is optimistic to gain sufficient high-redshift FRBs with the Five-hundred-meter Aperture Spherical radio Telescope (FAST) (Zhang 2018) and future Square Kilometer Array (SKA) (Fialkov & Loeb 2016). If high-redshift FRBs are observed with accurate redshift information from optical/infrared band, we can extend the $DM_{\text{IGM}} - z$ relation to the epoch of reionization (EoR). The relation can constrain the parameters in reionization model and the ionized fraction precisely.

The wide redshift range of IllustrisTNG gives us a chance to constrain the cosmic reionization history. We use the \tanh model given by Lewis (2008) (also applied

by Planck Collaboration et al. (2016)):

$$x_e(z) = \frac{f}{2} [1 + \tanh(\frac{y_{\text{re}} - y}{\Delta y})], \quad (11)$$

where x_e is ionized fraction. f is a normalized parameter for considering both hydrogen and helium and expressed as $f = 1 + f_{\text{He}} = 1 + n_{\text{He}}/n_{\text{H}}$. Typically $f \sim 1.08$, $y = (1+z)^{3/2}$, $y_{\text{re}} = (1+z_{\text{re}})^{3/2}$ and z_{re} is defined as the redshift at which $x_e = f/2$. $\Delta y = 1.5\sqrt{1+z_{\text{re}}}\Delta z$ and Δz reflects the duration of reionization. In the model of Lewis (2008), Δz is a fixed value. It was estimated with an upper limit of 1.3 at 95% confidence level in Planck Collaboration et al. (2016) redshift-symmetric case. Then we calculate $n_e(z)$ from

$$n_e(z) = \bar{n}_b(z) X_{\text{H}} x_e(z) \quad (12)$$

and

$$\bar{n}_b(z) = \frac{\Omega_b \rho_{\text{cr},0} (1+z)^3}{m_p}, \quad (13)$$

where $\rho_{\text{cr},0}$ is the critical density of universe. After taking $n_e(z)$ into equation (6), the theoretical value

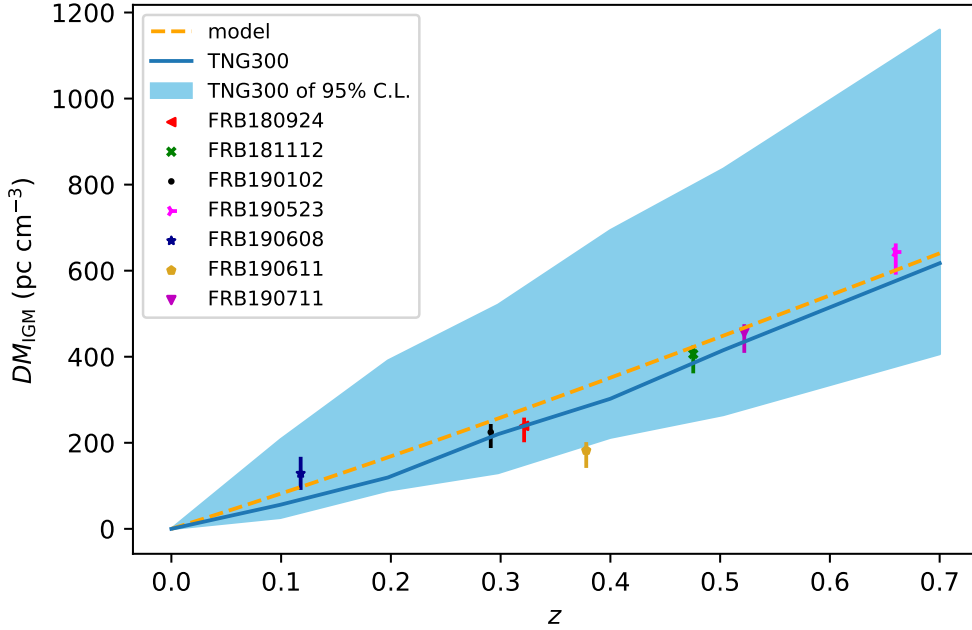


Figure 4. $DM_{\text{IGM}} - z$ (Macquart) relation from IllustrisTNG simulation and several localized FRBs. The orange dashed line is the model of equation (2). We take $f_{\text{IGM}} = 0.82 + 0.08z/0.9$, $f_e = 7/8$, and $X_{\text{e,H}} = X_{\text{e,He}} = 1$. The blue line is our result derived from TNG300 and the blue shaded region is the 95% confidence level. The two lines differ because the ionized fraction and IGM baryon fraction are different between the model and the simulation. We also show the DM_{IGM} value of several localized FRBs. In calculation, the DM_{MW} value is derived with the NE2001 model and DM_{host} is taken from Zhang et al. (2020) except FRB 190608 (taken from Chittidi et al. (2020)).

of DM_{IGM} can be obtained in this cosmic reionization model. Figure 5 gives the value of DM_{IGM} as a function of redshift up to $z \sim 9$. The blue line shows the derived DM_{IGM} from TNG300 simulation with 95% confidence region (blue region). Cosmic reionization affects both CMB power spectrum and kinematic Sunyaev-Zeldovich (kSZ) effect. We display the results from *Planck* data combined with the kSZ effect (Planck Collaboration et al. 2016) with the *tanh* model (see equation (11)) for comparison as well. The green line takes $z_{\text{re}} = 7.2$, which is the result from a uniform prior on the redshift at which the reionization ends (z_{end}). The orange line is the result from the prior $z_{\text{end}} > 6$ and it gives $z_{\text{re}} = 7.8$. The least-square-method fit (red line) indicates a very fast reionization process ($\Delta z = 0.05$) at $z_{\text{re}} = 5.95$ with the *tanh* model, which is also compatible with the model used by IllustrisTNG (Faucher-Giguère et al. 2009)². Therefore, high-redshift FRBs are promising probes of the cosmic reionization history.

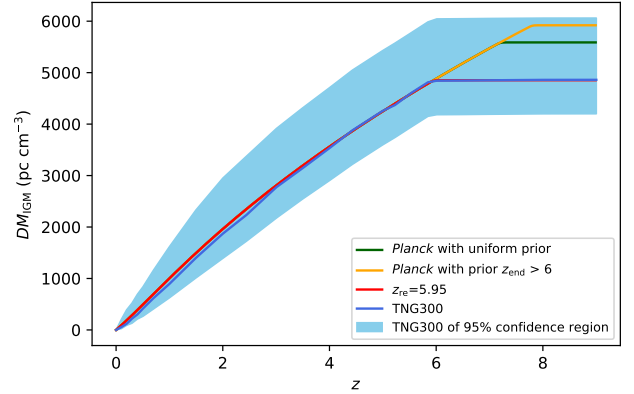


Figure 5. The blue line is our result and the red line is the best fit with the *tanh* model. For comparison, the value derived from *Planck* data is also shown (Planck Collaboration et al. 2016). The green line takes $z_{\text{re}} = 7.2$, which is the result from a uniform prior on the redshift at which the reionization ends. The orange line is the result from the prior $z_{\text{end}} > 6$ and it gives $z_{\text{re}} = 7.8$.

² Dec 2011 version, <https://galaxies.northwestern.edu/uvb-fg09/>

Meanwhile, we calculate the optical depth $\tau(z)$ of CMB contributed by IGM from

$$\tau(z) = \int_0^z \sigma_T n_e(z') dl_{\text{prop}}, \quad (14)$$

where $\sigma_T = 6.25 \times 10^{-25} \text{ cm}^2$ is the Thompson scattering cross section. The measurement of τ is changing for different instruments and we are curious whether FRBs may help. Using the electron number density derived from TNG300 simulation, we find that the total optical depth $\tau(z > 6) = 0.037^{+0.006}_{-0.004}$ with 95% confidence level. Figure 6 shows the value of $\tau(z)$ as a function of redshift from TNG300 simulation (blue line). The ionized electron fraction drops to zero before reionization so the optical depth saturates at high redshifts (Fialkov & Loeb 2016). The saturation value can be detected by high redshift FRBs which have no connection with CMB. The optical depth $\tau = 0.058 \pm 0.023$ (95% confidence level) from Planck result is shown as the orange region (Planck Collaboration et al. 2016). Considering the uncertainties, we find these two results are consistent with each other. Therefore, the DM of high-redshift FRBs provides an independent way to measure the optical depth of CMB, which can tightly constrain the cosmic reionization history. However, we must state that the resolution of *Planck* is 12 degrees which is much larger than that of FRBs. Comparing the two results with different resolution directly may be kind of inappropriate, however there is no need to decrease the resolution of FRBs.

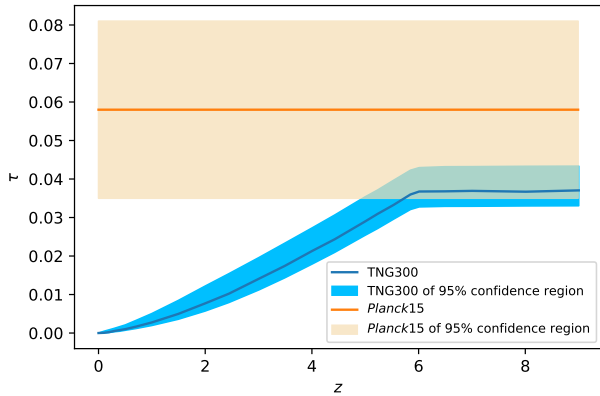


Figure 6. The blue line and shade region is our result with 95% confidence region. The orange line and region is *Planck* result with 95% confidence region (Planck Collaboration et al. 2016), which gives $\tau = 0.058 \pm 0.023$.

5. ESTIMATING THE REDSHIFTS OF NON-LOCALIZED FRBS

As mentioned before, there are only ten localized FRBs (Chatterjee et al. 2017; Bannister et al. 2019; Ravi et al. 2019; Prochaska et al. 2019; Marcote et al. 2020; Macquart et al. 2020), which means the redshifts for most FRBs are unknown. Assuming that the accurate DM_{IGM} is known, we check whether the redshift of FRB can be precisely derived from the $z - DM_{\text{IGM}}$ relation.

As mentioned in Section 2 and Section 3, we get $23 \times 10,000,000$ $DM_{\text{IGM}} - z$ data points (FRBs) in total (24 snapshots and 10,000,000 combinations). We divide the data points whose DM_{IGM} is between 0 and 6000 pc cm^{-3} into 150 bins (40 pc cm^{-3} in each bin) and calculate the mean redshift of these FRBs in each bin. The $z - DM_{\text{IGM}}$ relation is shown in Figure 7. The standard deviation of derived redshift is 0.74 at the pseudo-redshift 4.61 ($DM_{\text{IGM}} = 4000 \text{ pc cm}^{-3}$), which means the relative error is 16.1%. The small redshift standard deviations of FRBs whose DM_{IGM} are less than 4000 pc cm^{-3} show a good prospect for calculating pseudo-redshifts of non-localized FRBs.

We only take full snapshots at low redshifts, which means the redshifts of our simulated FRBs are restricted to some fixed redshifts such as 0.1, 0.2, 0.3, 0.4, 0.5, 0.7, 1 and 1.5. However, the standard deviation should not be larger when including mini snapshots because the standard deviation does not change for different sampling methods. What's more, the 40 pc cm^{-3} bin width can be taken as the systematic error during the estimation of DM_{halo} , DM_{host} and DM_{source} , which means it is even optimistic to derive the pseudo-redshift with a 'not very accurate' DM_{IGM} .

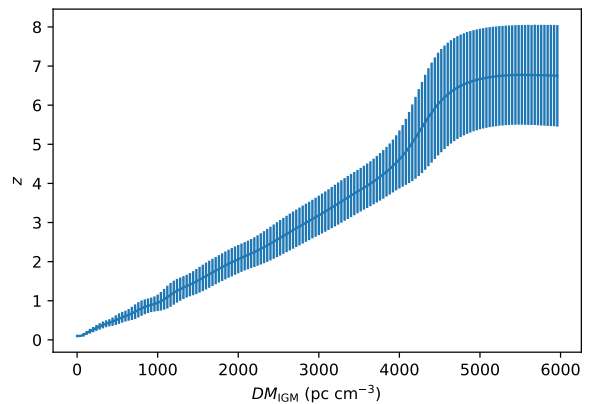


Figure 7. The $z - DM_{\text{IGM}}$ relation. The short blue lines show one standard deviation of each bin.

6. CONCLUSIONS

In this work, we derive DM_{IGM} of FRBs at the redshift range of $0 < z < 9$ from IllustrisTNG simulation.

We obtain $DM_{\text{IGM}} = 892_{-270}^{+721}$ pc cm⁻³ at $z = 1$. The DM_{IGM} value of localized FRBs are consistent with the derived $DM_{\text{IGM}} - z$ relation. At high redshifts $z > 5$, we show the scenario of probing the cosmic reionization history with FRBs. The *tanh* reionization model is used to fit the derived $DM_{\text{IGM}} - z$ relation at high redshifts. We find the reionization of IllustrisTNG universe occurs quickly at $z = 5.95$. This reionization model is compatible with the theoretical model used by the IllustrisTNG simulation (Faucher-Giguère et al. 2009). The optical depth of CMB is also derived from the IllustrisTNG simulation, which is consistent with that from Planck Collaboration et al. (2016). We try to limit the redshifts of non-localized FRBs with their DM_{IGM} . The standard deviation of pseudo-redshifts for non-localized FRBs is 16.1% for $DM_{\text{IGM}} = 4000$ pc cm⁻³.

The highest DM of observed FRB is 2596.1 ± 0.3 pc cm⁻³ and its nominal redshift is 2.1 (Bhandari et al. 2018; Caleb et al. 2018). It is predictable that there will be two orders of magnitude more FRBs in the next few years (Keane 2018). According to Fialkov & Loeb (2016) and Zhang (2018), FAST and SKA will have enough ca-

pability to detect FRBs out to $z = 14 \sim 15$. Therefore, FRBs will be a powerful and independent probe of the universe during epoch of reionization besides hydrogen 21-cm line. The future large sample of FRBs can be used to test our result about estimating redshifts for non-localized FRBs. What's more, most of previous works only considered the mean value of DM_{IGM} (equation 2) for cosmological constraints, while the scatter of it (Figure 2) which can degrade the cosmological constraints was not handled properly. Since IllustrisTNG shows a certain shape of the scatter, more authentic distributions of DM_{IGM} and DM_{host} can be used to test the FRB's capability of constraining cosmological parameters, such as Ω_{m} and Ω_{Λ} .

ACKNOWLEDGMENTS

We thank the anonymous referee for valuable comments. We thank Zhimei Tan, Lingrui Lin and Yichen Sun for helpful discussions and thank Dylan Nelson for his theoretical and technical help. This work is supported by the National Natural Science Foundation of China (grant U1831207).

REFERENCES

- Bannister, K. W., Deller, A. T., Phillips, C., et al. 2019, *Science*, 365, 565
- Bhandari, S., Keane, E. F., Barr, E. D., et al. 2018, *MNRAS*, 475, 1427
- Bhattacharya, M., Kumar, P. & Linder, E. V., 2020, arXiv: 2010.14530
- Caleb, M., Keane, E. F., van Straten, W., et al. 2018, *MNRAS*, 478, 2046
- Chatterjee, S., Law, C. J., Wharton, R. S., et al. 2017, *Nature*, 541, 58
- Chittidi, J. S., Simha, S., Mannings, A., et al. 2020, arXiv:2005.13158
- Cordes, J. M., & Lazio, T. J. W. 2002, arXiv e-prints, astro-ph/0207156
- Dai, J. P. & Xia, J. Q., 2020, arXiv: 2004.11276
- Deng, W., & Zhang, B. 2014, *ApJL*, 783, L35
- Dolag, K., Gaensler, B. M., Beck, A. M., et al. 2015, *MNRAS*, 451, 4277
- Faucher-Giguère, C.-A., Lidz, A., Zaldarriaga, M., et al. 2009, *ApJ*, 703, 1416
- Fialkov, A., & Loeb, A. 2016, *JCAP*, 2016, 004
- Gao, H., Li, Z., & Zhang, B. 2014, *ApJ*, 788, 189
- Inoue, S. 2004, *MNRAS*, 348, 999
- Ioka, K. 2003, *ApJL*, 598, L79
- Jaroszynski, M. 2019, *MNRAS*, 484, 1637
- Keane, E. F. 2018, *Nature Astronomy*, 2, 865
- Leung, C., Mena-Parra, J., Masui, K., et al. 2020, arXiv:2008.11738
- Lewis, A. 2008, *PhRvD*, 78, 023002
- Li, Z., Gao, H., Wei, J.-J., et al. 2019, *ApJ*, 876, 146
- Linder, E. V. 2020, *PhRvD*, 101, 103019
- Loeb, A., & Furlanetto, S. R. 2013, *The First Galaxies in the Universe*
- Lorimer, D. R., Bailes, M., McLaughlin, M. A., et al. 2007, *Science*, 318, 777
- Macquart, J.-P., Prochaska, J. X., McQuinn, M., et al. 2020, *Nature*, 581, 391
- Marcote, B., Nimmo, K., Hessels, J. W. T., et al. 2020, *Nature*, 577, 190
- Marinacci, F., Vogelsberger, M., Pakmor, R., et al. 2018, *MNRAS*, 480, 5113
- McQuinn, M. 2014, *ApJL*, 780, L33
- Muñoz, J. B., Kovetz, E. D., Dai, L., et al. 2016, *PhRvL*, 117, 091301
- Naiman, J. P., Pillepich, A., Springel, V., et al. 2018, *MNRAS*, 477, 1206
- Nelson, D., Pillepich, A., Springel, V., et al. 2018, *MNRAS*, 475, 624

- Peebles, P. J. E. 1968, *ApJ*, 153, 1
- Petroff, E., Hessels, J. W. T., & Lorimer, D. R. 2019, *A&A Rv*, 27, 4
- Pillepich, A., Nelson, D., Hernquist, L., et al. 2018, *MNRAS*, 475, 648
- Planck Collaboration, Adam, R., Aghanim, N., et al. 2016, *A&A*, 596, A108
- Planck Collaboration, Ade, P. A. R., Aghanim, N., et al. 2016, *A&A*, 594, A13
- Pol, N., Lam, M. T., McLaughlin, M. A., et al. 2019, *ApJ*, 886, 135
- Prochaska, J. X., Macquart, J.-P., McQuinn, M., et al. 2019, *Science*, 366, 231
- Prochaska, J. X., & Zheng, Y. 2019, *MNRAS*, 485, 648
- Ravi, V., Catha, M., D’Addario, L., et al. 2019, *Nature*, 572, 352
- Seager, S., Sasselov, D. D., & Scott, D. 2000, *ApJS*, 128, 407
- Springel, V., Pakmor, R., Pillepich, A., et al. 2018, *MNRAS*, 475, 676
- Vogelsberger, M., Genel, S., Springel, V., et al. 2014, *Nature*, 509, 177
- Walters, A., Weltman, A., Gaensler, B. M., et al. 2018, *ApJ*, 856, 65
- Wang, F. Y., Wang, Y. Y., Yang, Y.-P., et al. 2020, *ApJ*, 891, 72
- Wang, J.-S., Yang, Y.-P., Wu, X.-F., et al. 2016, *ApJL*, 822, L7
- Wang, Y. K., & Wang, F. Y. 2018, *A&A*, 614, A50
- Wei, J.-J., Li, Z., Gao, H., et al. 2019, *JCAP*, 2019, 039
- Wu, Q., Yu, H., & Wang, F.-Y. 2020, *ApJ*, 895, 33
- Yamasaki, S., & Totani, T. 2020, *ApJ*, 888, 105
- Yao, J. M., Manchester, R. N., & Wang, N. 2017, *ApJ*, 835, 29
- Yu, H., & Wang, F. Y. 2017, *A&A*, 606, A3
- Zel’dovich, Y. B., Kurt, V. G., & Syunyaev, R. A. 1969, *Soviet Journal of Experimental and Theoretical Physics*, 28, 146
- Zhang, B. 2018, *ApJL*, 867, L21
- Zhang, B. 2020, *ApJL*, 890, L24
- Zhang, G.-Q., Yu, H., He, J. H. & Wang, F.-Y. 2020, *ApJ*, 900, 170
- Zhao, Z. et al., 2020, arXiv: 2006.01450
- Zhao, Z. Y., Zhang, G. Q., Wang, Y. Y. & Wang, F. Y., 2020, arXiv: 2010.10702
- Zheng, Z., et al., 2014, *ApJ*, 797, 71
- Zhou, B., Li, X., Wang, T., et al. 2014, *PhRvD*, 89, 107303
- Zhu, W. S. & Feng, L. L., arXiv: 2011.08519